https://dx.doi.org/10.1016/j.mtcomm.2021.102906

Abrasive wear behaviour of TiC-strengthened eutectic high chromium cast iron composites

R.N. Jia[a,b], T.Q. Tu[a,b], K.H. Zheng[a,b], Z.B. Jiao[c], Z.C. Luo[a,b*]

[a]Institute of Materials and Processing, Guangdong Academy of Science, Guangzhou, China, 510000

[b]Guangdong Provincial Key Laboratory of Metal Toughening Technology and Application, Guangzhou, China, 510000

[c]Department of Mechanical Engineering, The HongKong Polytechnic University, Hong Kong, China, 999077

*Corresponding author, email: luozhichao@gimp.gd.cn

Abstract:

This study investigates abrasive wear behavior of TiC-strengthened eutectic high chromium cast iron (eHCCI) composites. The effect of TiC content and heat treatment on the wear properties of eHCCIs before and after heat treatment was investigated by combining the three-body abrasive wear and micro-scratch tests. The experimental results show that the as-cast TiC-reinforced eHCCIs exhibited superior abrasive resistance, which was originated from the synergic contribution of ductile austenitic matrix and hard carbides. However, the introduction of TiC particles significantly reduced the wear resistance of the eHCCIs after heat treatment due to the low ductility of martensite matrix.

Keywords: Abrasive wear; High chromium cast iron; TiC; Composites; Wear resistance.

Introduction

The high chromium cast irons (HCCIs) with a composition range of 12-30 wt.% Cr and 2.0-4.3 wt.% C have attracted intensive research interests due to their favorable combination of corrosion and wear resistance [1-9]. Such excellent properties make HCCIs candidate wear-resistant materials for the application in many areas, including mining, cement production, and refractory industries. It is believed that exceptional wear resistance of HCCIs is caused by the formation of a high-volume fraction of M_7C_3 carbides (1200-1600 HV in hardness) in the microstructure.

Generally, a high-volume fraction of M_7C_3 by increasing the Cr and C contents in hypereutectic HCCIs results in improved wear resistance of materials. However, coarse primary carbides precipitate during the solidification of hypereutectic HCCIs[3, 10-15]. These coarse primary carbides lower the fracture toughness and reduce the wear resistance of HCCIs[14]. Many investigations have been applied to refine the solidification structure and improve the mechanical and wear properties of hypereutectic HCCIs[3, 5, 11, 13, 15-20].

For comparison, the hypoeutectic HCCIs contain a low fraction of carbides, and the as-cast microstructure contains primary austenite phase and eutectic M_7C_3 carbides [8]. The toughness of hypoeutectic HCCIs is higher than the hypereutectic HCCIs, but their hardness and wear resistance is relatively low. The HCCIs with a eutectic composition, i.e. eHCCIs, possess a good balance of hardness and toughness. However, the volume fraction of M_7C_3 carbides is limited due to the narrow composition range of eutectic reaction for a given chromium content.

In this work, we propose a novel alloying design strategy for the HCCIs. That is, fine MC carbides were introduced to the eHCCIs to obtain a high carbide fraction. Accordingly, the eHCCI matrix strengthened with various volume fractions of TiC were designed and fabricated by an in-situ solidification method. The effects of TiC content and heat treatment on the microstructure and wear properties of the composites were investigated. Contrary to the conventional wisdom [21, 22], we found that the heat treatment reduces the abrasive wear property of the composites, even though the hardness was improved. The physical correlation between the mechanical properties and the abrasive wear resistance was investigated.

Furthermore, micro-scratch tests were applied to study the abrasive wear mechanisms of the composites. Other than the scratch hardness, it has also been reported that the scratch ductility controls the tendency to undergo material removal during scratch[23-29]. In this work, the scratch hardness and ductility of the TiC-reinforced eHCCIs were also obtained from the micro-scratch test under the same loading force as the conventional abrasive wear test. The abrasive wear mechanisms of these composites were critically discussed.

Materials and methods

The materials used for this study were fabricated in a vacuum melting furnace. The solutionization treatment was carried out at 1123 K for 4 h, followed by air cooling to room temperature. The temper treatment was conducted at 773 K, followed by furnace cooling down to room temperature. Table 1 shows the chemical compositions of the samples. The as-received (as cast??) and heat-treated samples were noted

hereafter as C0- C3 and H0-H3, respectively.

Prior to the microstructure examination, the samples were polished by abrasive paper and diamond paste. Vibration polishing was performed in the colloidal silica suspension (50 nm) for 4 h. The morphology of the worn surface was investigated by scanning electronic microscope (SEM Nova NanoSEM 430) at 20 V. The phase constitution of different samples was identified by high-resolution X-ray diffractometer (XRD Smartlab) at a stable voltage of 40 kV. The X-ray scanning angle was from 30° to 90°, with a speed of 0.01 degree per step. 3-D profilometer (Operating Instructure of 3D Profile, Bruker) was used to evaluate the worn surface after the micro-scratch test.

The Rockwell hardness of samples was measured (5 times for each sample) by HR-150A with a bearing force of 500 g and a holding time of 10 s. Before the three-body abrasive wear tests, the samples were cleaned carefully in ethanol. The friction and wear tests were performed on a three-body abrasive wear machine in a load of 3 Kg at room temperature. The white corundum sand with a mean size of 0.22 mm was adopted as abrasive particles. The test configurations and specimen geometries can be found in our previous paper [13]. After a 0.5 h of pre-wear, the weight changes of the specimens were recorded every hour. The mass of samples was measured by a METTLER TOLEDO balance (with a sensitivity of 0.1 mg) before and after wear test. The wear rate was characterized by the ratio of volume loss to sliding distance.

The scratch tests were carried out by MET-4000 Multifunctional material surface

analysis machine at room temperature. A smooth conical shape (120°) diamond indenter was used. The selected loading forces ranged from 10 to 200 N. Figure 1 shows the cross-section of a scratch formed by the cone indenter. The d and a were defined as the depth of penetration from the original surface and the corresponding groove half-width, respectively. And the a' is the half-width of the whole groove. The A1, A2 and Av are the area of the three zones as shown in Fig. 1.

Results

Figure 2 shows the microstructure of the TiC-strengthened eHCCIs in the as-cast state. It can be seen that the microstructure consists of two kinds of carbides. The rod-like grey particles are eutectic M_7C_3 carbides, and the black particles are TiC particles, as proved by the EDS results. No coarse primary M_7C_3 particles can be observed in all the HCCI specimens, as shown in Fig. 2. Figure 3 shows the EBSD IPF figures of the as-cast composites. It reveals that the as-cast composites consists of austenite matrix, M_7C_3, and TiC. Therefore, the eutectic HCCIs strengthened by TiC particles were successfully prepared in the present work.

The volume fractions and sizes of M_7C_3 and TiC were measured by Image Pro-plus 6.0. Figure 4 shows the Ti-dependent carbide volume fraction and carbide size. It shows that the volume fraction of M_7C_3 carbide decreases from 23 % to 18 % with increasing Ti and C contents, while the volume fraction of TiC increases from xx to 10%. Therefore, the total volume fraction of carbides increases slightly with increasing Ti and C contents as shown in Fig. 4a. Furthermore, the mean size of M_7C_3 decreases as shown in Fig. 4b.

Figure 5 shows the XRD patterns of the TiC-strengthened eutectic HCCIs in the as-cast and heat-treated states. The as-cast HCCIs contain austenite matrix and two categories of carbide (M_7C_3 and TiC) as shown in Fig. 5a. The XRD results are consistent with the EBSD results as shown in Fig. 3. After heat treatment, the matrix consists of dominant martensite and minor retained austenite, together with the carbides, as shown in Fig. 5b.

The wear resistance of TiC-strengthened eHCCIs was investigated by three-body abrasive wear test. Figure 6 shows that the wear rate of the as-cast composites decreases with increasing volume fraction of TiC. By contrast, the wear rate of the heat-treated composites increases with TiC content. It means that the introduction of TiC particles is detrimental to the wear property of the composites after heat treatment. Specifically, with the addition of 10 vol.% TiC, the wear rate of the as-cast eutectic HCCI decreases from 8 to 5 $cm^3/cm \cdot 10^{-8}$. When the reciprocal of wear rate was used to present the wear resistance, the improvement of wear resistance by the introduction of 10 vol.% TiC can be as high as 60% for the as-cast composites. On the other hand, the wear resistance of TiC-free HCCIs can be effectively improved by the heat treatment. However, for the TiC-strengthened HCCIs, the heat treatment causes a significant increment of wear rate as shown in Fig. 6.

Figure 7 shows the SEM images of the worn surface of the sample after three-body abrasive wear tests. The pits, grooves, and scars can be observed in the worn surface as shown by the arrows in Fig. 7. The bright zones in Fig. 7 were caused by accumulations of materials as a result of the severe plastic deformation. As the TiC

volume fraction increases, the amount of bright zones increases and the directions of grooves were changed by the presence of hard phase as shown in Fig. 7(b-d). The heat-treated samples show similar wear behaviour with the as-cast samples as shown in Fig.7(h-k).

To further explore the combined effect of TiC addition and heat treatment on the wear resistance of composites, we performed the micro-scratch wear experiments. After the scratch tests, the groove profiles were obtained. In this work, the dent area Av was used to evaluate the wear properties of HCCIs. Figure 8 shows the load-dependent dent area of the HCCIs before and after heat treatment. It can be seen that the dent area increases with the load force. As the loading force exceeds 30 N, the dent area of heat-treated specimens becomes higher than that of as-cast specimens. Furthermore, the dent area is used to represent the wear rate, the wear rate of as-cast composites can be reduced by the introduction of TiC particles. However, the wear rate of heat-treated composites increases with TiC additions, especially when the loading force is higher than 60 N. The present micro-scratch results are consistent with the three-body abrasive test results as shown in Fig. 6.

Figure 9 shows the SEM image of HCCIs after micro scratch test at a loading force of 60 N. Many cracks emerged on both the M_7C_3 and TiC particles as shown in Fig. 9(a-d). It can be noted that the matrix can prevent crack propagation from the carbides. Different from the as-cast samples, the scratch surface of the heat-treated HCCIs display typical delamination wear feature as shown in Fig. 9(h-k). The crack can propagate to the substrate, and thereby a large amount of materials has been removed

by scratching.

To describe the scratching resistance, the scratch hardness (Hs) and ductility (δc) proposed by Williams and Hokkirigawa were presented. The Hs can be expressed as[27, 29]:

$$Hs = \frac{2F}{\pi a'^2} \tag{1}$$

where F is the normal force and a' is the half-width of the groove as shown in Fig. 1.

The calculation of δc can be used the following empirical equations[27, 30]:

$$f = \frac{Av - (A1 + A2)}{Av} \tag{2}$$

$$f = (1 - 4\delta c) \cdot \left\{ 1 - \exp\left[-0.11 \left(\frac{\delta}{\delta c} \right)^3 \right] \right\} \tag{3}$$

where f is the material removal fraction, δ is the normalized depth calculating by d/a, and δc is the scratch ductility, whose value should be less than 0.25. Then the Hs and δc of HCCIs can be calculated.

Figure 10 shows the calculation results. The scratching profiles under a loading force of 30 N, which is close to the force of the abrasive wear test, were used for the calculation. It can be noted that both the Rockwell and scratch hardnesses increase with the TiC addition as shown in Fig. 10a. A linear relationship can be obtained (with $R^2 = 0.99$)

$$HRC = (8.3 \pm 0.2) \times 10^{-3} \times Hs \tag{4}$$

Figure 10b shows the scratch ductility and hardness of eight specimens. It clearly shows that there is a trade-off between the scratch ductility and hardness. That is, the scratch ductility decreases with the increased scratch hardness. It also shows that the scratch ductility of heat-treated composites is lower than that of as-cast composites. Furthermore, the as-cast composites reveals a better combination of scratch ductility and hardness than the heat-treated composites as shown in Fig. 10b.

Discussion

In this work, TiC-strengthed eutectic HCCI composites were designed and fabricated. The effects of TiC volume fraction and heat treatment on the wear properties of composites were investigated by three-body abrasive wear and micro-scratch tests.

For the conventional HCCIs, the carbide volume fraction (CVF) increases with Cr and C content, which follows an empirical linear equation[1]:

$$CVF = 14.05 \cdot C + 0.43 \cdot Cr - 0.22 \quad (5)$$

where the ω_C and ω_{Cr} are the weight fractions of C and Cr, respectively. Based on Eq. (5), the CVF of the present base steel (C0 and H0) is 0.33, which is higher than the measurement results as shown in Fig. 4a. Furthermore, the CVF in the present HCCIs increases slightly with carbon content as shown in Fig. 4a. Figure 11 shows the phase constitutions of two HCCIs with and without Ti during cooling. In the liquid phase containing Ti and C, the TiC phase is formed first. At the temperature around 1573 K, the eutectic reaction occurs where the liquid phases transform to austenite and M_7C_3 as shown in Fig. 11.

It has been reported that the matrix of as-cast HCCIs has an austenitic

microstructure[31]. During the soaking at 1223-1333 K, the precipitation of Cr-rich secondary carbides occurs in the austenite matrix. The reduced Cr and C contents in the alloy destabilize the austenitic matrix, allowing it to transform to martensite during the subsequent cooling. Therefore, the destabilization treatment results in a dominant martensite matrix as shown in Fig. 5b. For the TiC-free HCCIs, the heat treatment significantly improves their hardness (Fig. 10a), and hence the abrasive wear properties of H0 are higher than that of C0 as shown in Fig. 6.

For the as-cast composites, the introduction of TiC particles can effectively improve the hardness as shown in Fig. 10a. Such improvements can be due to the increased amount of hard MC carbides, the refinement of M_7C_3, and the increased total volume fraction of carbides (Fig. 4). However, the heat treatment causes a significant reduction of the abrasive properties for the composites, especially when the TiC volume fraction is high (Fig. 6). It should also be noted that the heat treatment increases the Rockwell hardness of the HCCIs with no or a low volume fraction of TiC but reduces the Rockwell hardness of the HCCIs with a high volume fraction of TiC (Fig. 10).

It is believed that the ductile austenitic matrix makes the as-cast Ti-reinforced HCCI composites more abrasion resistant under the present experimental conditions. During the abrasive wear process, the austenite phase can flow more easily without fracture under the shear forces applied by the abrasive particles. The plastic deformation of the matrix can effectively dissipate the mechanical energy into a larger volume and cause less damage per unit volume. For comparison, the martensite matrix is brittle. As a

result, the energy dissipation is realized by the fracture of the matrix and carbides. Figrue 12 shows the indentations of three specimens after the Viker hardness test. It can be seen that there is no cracks in C3. For comparison, the cracks can be observed on both matrix and particles in H2 and H3. Accordingly, it suggests that the soft and ductile matrix can support the carbides after their fracture and thereby improve the wear resistance of HCCIs. In contrast, the introduction of brittle martensite may cause a high wear rate of the HCCIs.

In this work, micro-scratch experiments were applied to investigate the wear properties of the HCCIs. The intrinsic scratch response of the material can be assessed, which is critical to understand the complexity of abrasive wear. Micro-scratch experiments have been applied to investigate the wear behavior of various materials including high-strength steels, Ni-base alloys, Hadfield steel, and high entropy steels [23, 25-27]. It has been reported that the fraction of material removed in a groove (f, in Eq. 2) can assist in defining the dominant wear mechanism operating in the wear process [27, 32]. Values of about 02 - 0.4 imply a plowing mechanism, while values of more than 0.7 are indicative of a cutting mechanism. In this work, it was found the f values of HCCIs after heat treatment was higher than that of the as-cast HCCIs. It reveals that the cutting becomes a dominant material removal mechanism for the HCCIs after heat treatment. This was consistent with the groove morphology observation (Fig. 9) that the results of the plowing mechanisms to the smooth scratch surface in the as-cast HCCIs, while delamination and large cracks were found in the heat-treated HCCIs due to the strong resistance of hard matrix against the scratch.

Generally, plasticity and hardness are the key factors that affect the wear resistance of materials. The scratch hardness and ductility were obtained as shown in Fig. 10b. It has also been reported that the combination of scratch ductility and hardness deciding the wear loss during the micro-scratch test[28, 30]. In this work, the scratch results under 30 N were compared with the three-body wear test results under a similar load of 3 kg. Figure 13 shows the correlation of abrasive wear rate and the reciprocal of the multiplication of scratch hardness and ductility of eight specimens. It can be seen that the wear rate has a linear relationship with the reciprocal of $H_s \cdot \delta_c$.

The good correlation between the abrasive wear test and the scratch test results indicates that the micro-scratch experiment offers a fast method to quantify the abrasion resistance of materials. Although the three-body abrasive test provides useful data on the relative wear rate, it limits to the test conditions. The actual deformation and damage processes for various loading conditions can be investigated readily by the micro-scratch tests.

Conclusions

This work investigates the effect of TiC addition and heat treatment on the microstructure and abrasive wear behavior of eutectic HCCIs. Three-body abrasive and micro-scratch experiments were conducted on the TiC-reinforced eHCCIs composites. The following conclusions are drawn.

(1) The as-cast composites consist of an austenitic matrix, M_7C_3, and TiC carbides. With increasing TiC content, the carbide volume fraction increases and the size of M_7C_3 is slightly refined. After heat treatment, the matrix transforms to martensite.

(2) For the as-cast composites, the introduction of TiC significantly improves the abrasive wear properties. However, the abrasive wear properties decrease with TiC additions for the heat-treated composites even though the hardness is improved by the addition of TiC particles. Furthermore, when the volume fraction of TiC is higher than 6%, the abrasive wear property of the as-cast composites is higher than those after heat treatment.

(3) For the as-cast composites, the downward trend of scratch ductility with TiC content is not obvious. For comparison, the scratch ductility of heat-treated HCCIs is lower than that in the as-cast state and decreases significantly with the introduction of TiC particles.

(4) There is a linear correlation between the three-body abrasive wear rate with the reciprocal of the multiplication of scratch hardness and ductility. The superior abrasive wear resistance of the as-cast composites is originated from the synergic contribution of ductile austenitic matrix and hard carbides. The reduced abrasive wear property of the heat-treated composites can be attributed to the low ductility of martensite.

Acknowledgment

The authors acknowledge the financial support from Guangdong Academy of Science (2020GDASYL-20200103134), National Natural Science Foundation of China (51901049 and 51801169), Guangzhou Municipal Science and Technology Project (No. 202007020007, 201807010079 and 201907010026), Guangdong Provincial Science and Technology Cooperation Project (2018A050506055). Z.C. Luo

acknowledges Prof. M.X. Huang in the University of Hong Kong for providing the assess to the Thermal-calc software.

Reference

[1] Ö.N. Doğan, J.A. Hawk, G. Laird, Solidification structure and abrasion resistance of high chromium white irons, Metallurgical and Materials Transactions A, 28 (1997) 1315-1328.

[2] A. Wiengmoon, T. Chairuangsri, A. Brown, R. Brydson, D.V. Edmonds, J.T.H. Pearce, Microstructural and crystallographical study of carbides in 30wt.%Cr cast irons, Acta Materialia, 53 (2005) 4143-4154.

[3] X. Zhi, J. Xing, H. Fu, B. Xiao, Effect of niobium on the as-cast microstructure of hypereutectic high chromium cast iron, Materials Letters, 62 (2008) 857-860.

[4] R.J. Chung, X. Tang, D.Y. Li, B. Hinckley, K. Dolman, Abnormal erosion–slurry velocity relationship of high chromium cast iron with high carbon concentrations, Wear, 271 (2011) 1454-1461.

[5] K. Shimizu, K. Kusumoto, X. Yaer, Y. Zhang, M. Shirai, Effect of Mo content on erosive wear characteristics of high chromium cast iron at 1173K, Wear, 376-377 (2017) 542-548.

[6] K.D. Tozetti, E. Albertin, C. Scandian, Abrasive size and load effects on the wear of a 19.9% chromium and 2.9% carbon cast iron, Wear, 376-377 (2017) 46-53.

[7] X. Chong, M. Hu, P. Wu, Q. Shan, Y.H. Jiang, Z.L. Li, J. Feng, Tailoring the anisotropic mechanical properties of hexagonal M7X3 (M=Fe, Cr, W, Mo; X=C, B) by multialloying, Acta Materialia, 169 (2019) 193-208.

[8] I. Fordyce, M. Annasamy, S.D. Sun, D. Fabijanic, S.C. Gallo, M. Leary, M. Easton, M. Brandt, The effect of heat treatment on the abrasive and erosive wear behaviour of laser metal deposited Fe–28Cr–2.7C alloy, Wear, 458-459 (2020) 203410.

[9] A.E.d. Silva, I.N.R.d. Melo, I.P. Pinheiro, L.R.d. Silva, Characterisation and machinability of high chromium hardened white cast iron with and without the addition of niobium, Wear, 460-461 (2020) 203463.

[10] J. Zhifu HUANG, ong XING, Anfeng ZHANG, Microstructure and Property of Hypereutectic High Chromium Cast Iron Prepared by Slope Cooling Body-Centrifugal Casting Method, J. Mater. Sci. Technol., 22 (2006) 775-778.

[11] R.J. Chung, X. Tang, D.Y. Li, B. Hinckley, K. Dolman, Effects of titanium addition on microstructure and wear resistance of hypereutectic high chromium

cast iron Fe–25wt.%Cr–4wt.%C, Wear, 267 (2009) 356-361.

[12] R.J. Chung, X. Tang, D.Y. Li, B. Hinckley, K. Dolman, Microstructure refinement of hypereutectic high Cr cast irons using hard carbide-forming elements for improved wear resistance, Wear, 301 (2013) 695-706.

[13] L. Zhichao, J.P. Ning, J. Wang, K.H. Zheng, Microstructure and wear properties of TiC-strengthened high-manganese steel matrix composites fabricated by hypereutectic solidification, Wear, 432-433 (2019) 202970.

[14] Y. Pei, R. Song, Y. Zhang, L. Huang, C. Cai, E. Wen, Z. Zhao, P. Yu, S. Quan, S. Su, C. Chen, The relationship between fracture mechanism and substructures of primary M7C3 under the hot compression process of self-healing hypereutectic high chromium cast iron, Materials Science and Engineering: A, 779 (2020) 139150.

[15] Y. Zhang, R. Song, Y. Pei, E. Wen, Z. Zhao, The formation of TiC–NbC core-shell structure in hypereutectic high chromium cast iron leads to significant refinement of primary M7C3, Journal of Alloys and Compounds, 824 (2020) 153806.

[16] A. Bedolla-Jacuinde, R. Correa, J.G. Quezada, C. Maldonado, Effect of titanium on the as-cast microstructure of a 16%chromium white iron, Materials Science and Engineering: A, 398 (2005) 297-308.

[17] C. Scandian, C. Boher, J.D.B. de Mello, F. Rézaï-Aria, Effect of molybdenum and chromium contents in sliding wear of high-chromium white cast iron: The relationship between microstructure and wear, Wear, 267 (2009) 401-408.

[18] X. Qi, Z. Jia, Q. Yang, Y. Yang, Effects of vanadium additive on structure property and tribological performance of high chromium cast iron hardfacing metal, Surface and Coatings Technology, 205 (2011) 5510-5514.

[19] H.K. Zeytin, H. Yildirim, B. Berme, S. Duduoĝlu, G. Kazdal, A. Deniz, Effect of Boron and Heat Treatment on Mechanical Properties of White Cast Iron for Mining Application, Journal of Iron and Steel Research, International, 18 (2011) 31-39.

[20] J.J. Penagos, J.I. Pereira, P.C. Machado, E. Albertin, A. Sinatora, Synergetic effect of niobium and molybdenum on abrasion resistance of high chromium cast irons, Wear, 376-377 (2017) 983-992.

[21] G.W. Stachowiak, A.W. Batchelor, 11 - Abrasive, Erosive and Cavitation Wear, in: G.W. Stachowiak, A.W. Batchelor (Eds.) Engineering Tribology (Third Edition), Butterworth-Heinemann, Burlington, 2006, pp. 501-551.

[22] K. Hokkirigawa, K. Kato, Z.Z. Li, The effect of hardness on the transition of the abrasive wear mechanism of steels, Wear, 123 (1988) 241-251.

[23] X. Xu, S. van der Zwaag, W. Xu, The scratch and abrasive wear behaviour of a tempered martensitic construction steel and its dual phase variants, Wear, 358-359 (2016) 80-88.

[24] L.Z. Yun Wang, Yanjie Hu, Chunzhong Li, Comparative Study on Optical Properties and Scratch Resistance of Nanocomposite Coatings Incorporated with Flame Spray Pyrolyzed Silica Modified via in-situ Route and ex-situ Route, J. Mater. Sci. Technol., 32 (2016) 251-258.

[25] P.C. Machado, J.I. Pereira, J.J. Penagos, T. Yonamine, A. Sinatora, The effect of in-service work hardening and crystallographic orientation on the micro-scratch wear of Hadfield steel, Wear, 376-377 (2017) 1064-1073.

[26] A. Shugurov, A. Panin, A. Dmitriev, A. Nikonov, The effect of crystallographic grain orientation of polycrystalline Ti on ploughing under scratch testing, Wear, 408-409 (2018) 214-221.

[27] N. Haghdadi, T. Guo, A. Ghaderi, P.D. Hodgson, M.R. Barnett, D.M. Fabijanic, The scratch behaviour of AlXCoCrFeNi (x=0.3 and 1.0) high entropy alloys, Wear, 428-429 (2019) 293-301.

[28] S. Xiao, K.A. Laux, H. Wang, F. Hu, H.-J. Sue, Physical correlation between abrasive wear performance and scratch resistance in model polyurethane elastomers, Wear, 418-419 (2019) 281-289.

[29] J.A. Williams, Analytical models of scratch hardness, Tribology International, 29 (1996) 675-694.

[30] A. Ghaderi, G. Saha, T. Guo, D. Fabijanic, M.R. Barnett, Material wear map for ground-engaging steels based on scratch tests, Wear, 404-405 (2018) 153-165.

[31] T.C. A.Wiengmoon, N.Chomsang, N.Poolthong, J.T.H.Pearce, Effects of Heat Treatment on Hardness and Dry Wear Properties of a Semi-Solid Processed Fe-27 wt pct Cr-2.9 wt pct C Cast Iron, J. Mater. Sci. Technol., 24 (2008) 330-334.

[32] L.A. Franco, A. Sinatora, Material removal factor (fab): A critical assessment of its role in theoretical and practical approaches to abrasive wear of ductile materials, Wear, 382-383 (2017) 51-61.

Tables

Table 1. Chemical composition and number of samples.

	Chemical composition (wt.%)	As-cast	Heat treatment
1	Fe-26Cr-**3.2C**-0.4Mn-0.8Si-1Ni	C0	H0
2	Fe-26Cr-**3.2C**-0.4Mn-0.8Si-1Ni-(**0.4C-1.6Ti)**	C1	H1
3	Fe-26Cr-**3.2C**-0.4Mn-0.8Si-1Ni-(**0.8C-3.2Ti)**	C2	H2
4	Fe-26Cr-**3.2C**-0.4Mn-0.8Si-1Ni-(**1.2C-4.8Ti)**	C3	H3

Figures

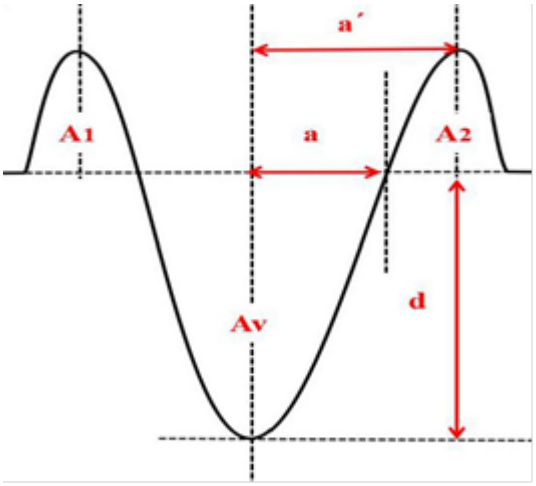

Fig. 1. Cross-section of an ideal scratch. The d and a were defined by the depth of penetration from the original surface and the corresponding groove half-width, respectively. The a' is the half-width of the whole groove, and $A1$, $A2$ and Av are the area of three zones.

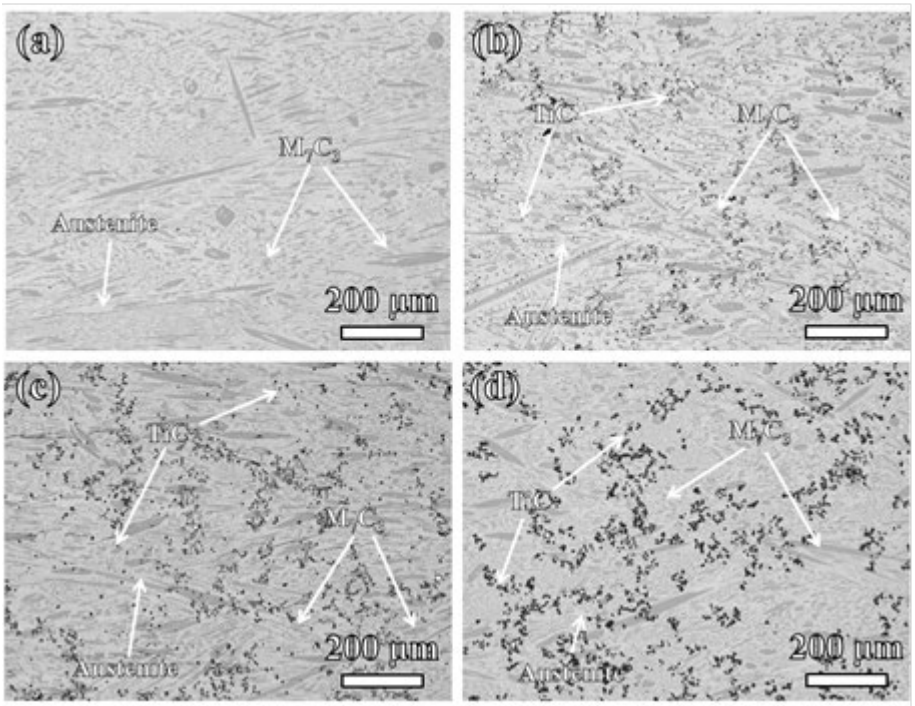

Fig. 2. SEM images of the as-cast composites: (a) C0, (b) C1, (c) C2, and (d) C3.

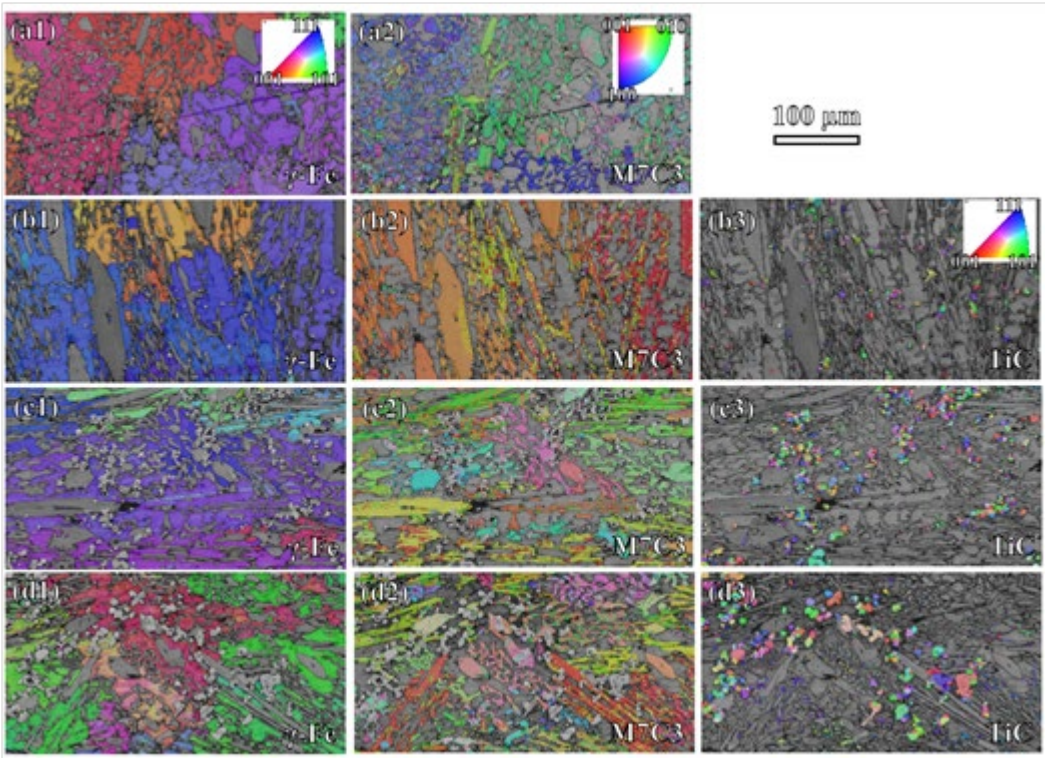

Fig. 3. EBSD inverse pole figures (IPF) of the as-cast composites: (a1-a2) C0,(b1-b3) C1, (c1-c3) C2, and (d1-d3) C3

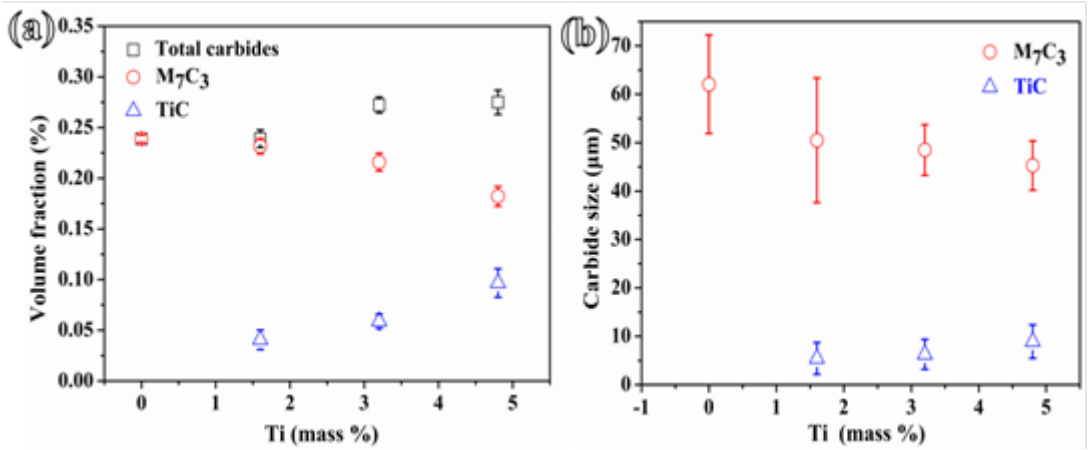

Fig. 4. The volume fractions (a) and sizes (b) of M_7C_3 and TiC carbides in the as-cast HCCIs.

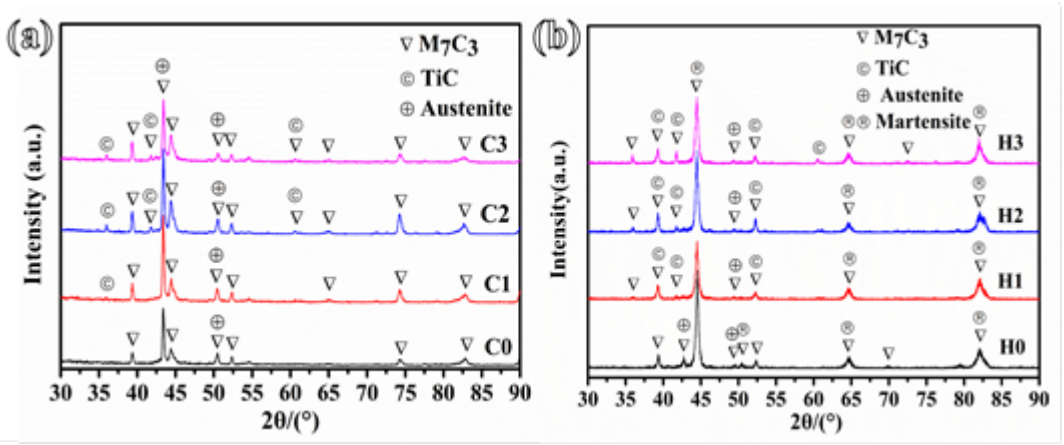

Fig. 5. XRD patterns of TiC-strengthened HCCIs: (a) as-cast and (b) after heat treatment.

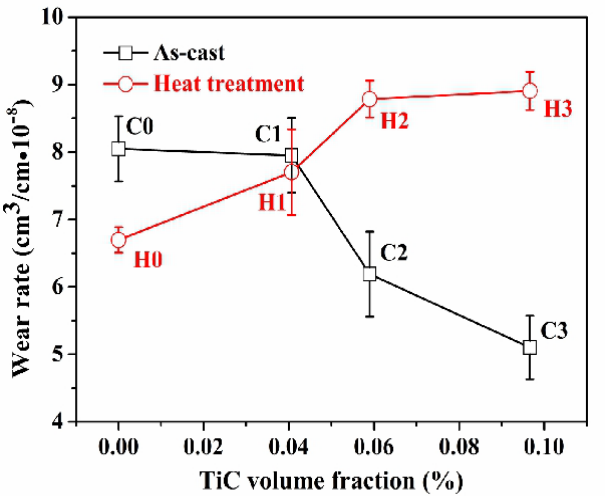

Fig. 6. The abrasive wear rate of the as-cast and heat-treated composites.

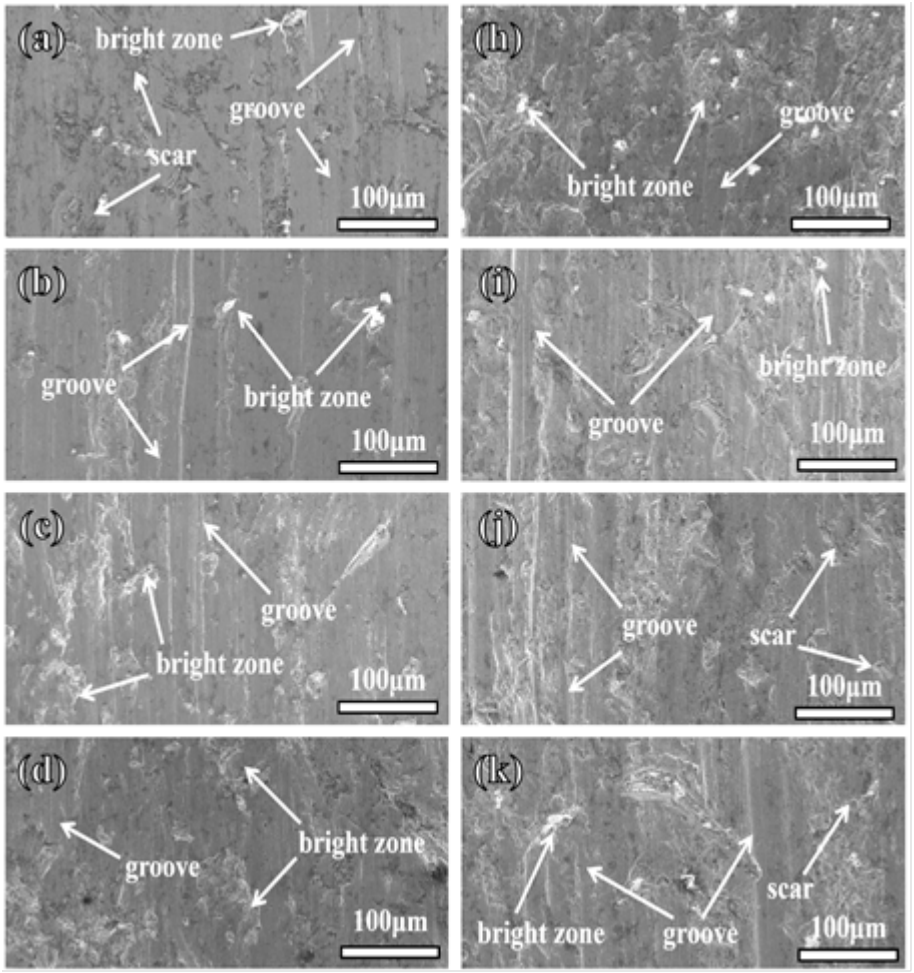

Fig. 7. The worn surface of composites after abrasive wear tests: (a-d) C0, C1 C2, and C3; (e-k) H0, H1, H2, and H3.

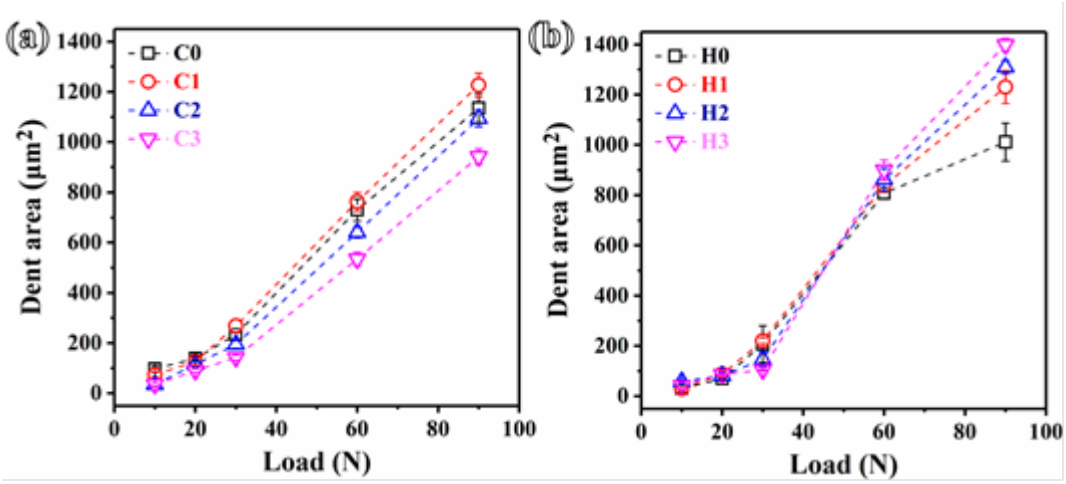

Fig. 8. The dent area under different micro scratch loads: (a) the as-cast composites and (b) the heat-treated composites.

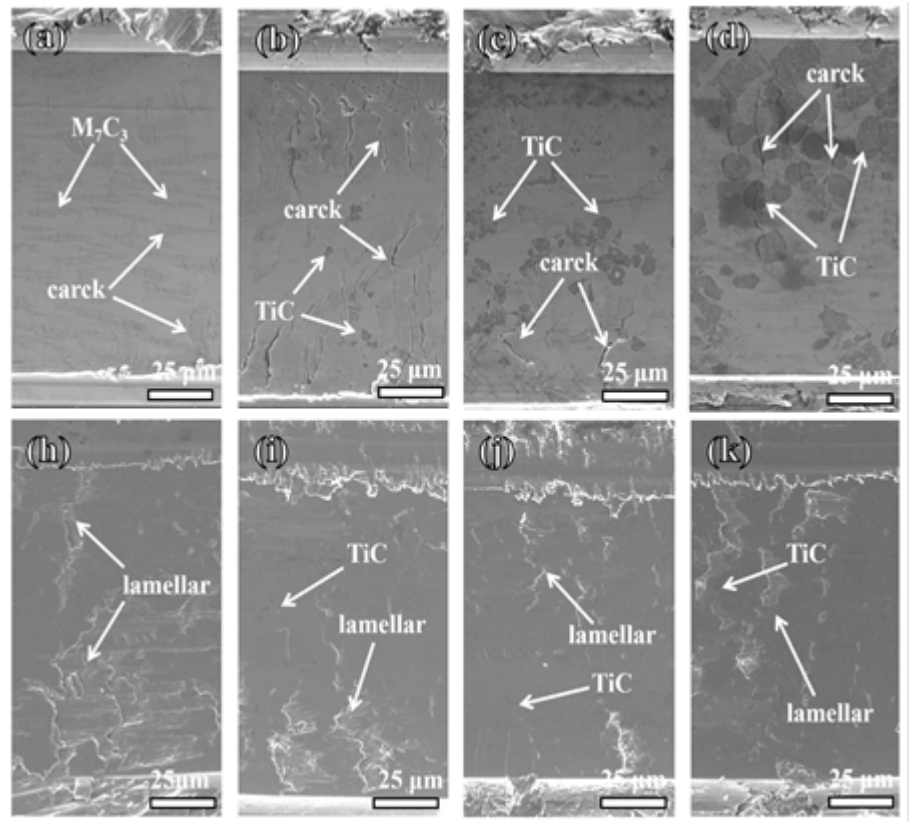

Fig. 9. The groove morphology after scratching tests at 60 N: (a-d) C0, C1, C2 and (C3); (h-k) H0, H1, H2 and H3.

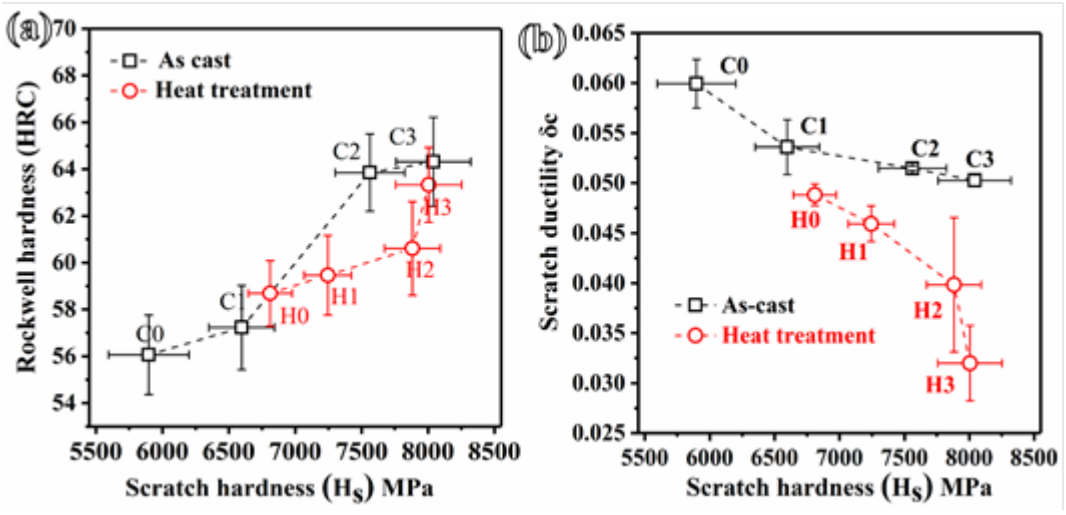

Fig. 10. Scratch hardness and scratch ductility of composites: (a) the scratch hardness and Rockwell hardness and (b) the scratch hardness and ductility.

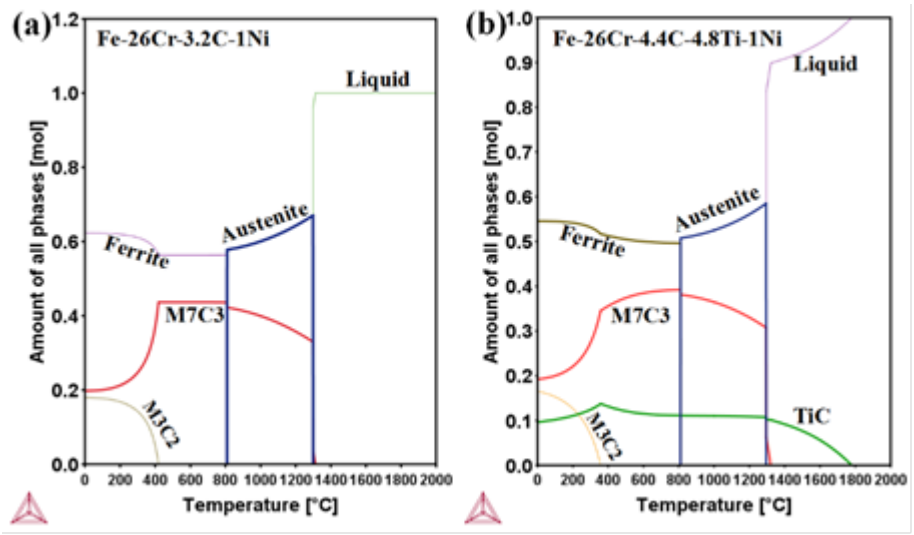

Fig. 11. Phase constitutions during cooling of two HCCIs (in wt.%): (a) Fe-26Cr-3.2C-1Ni and (b) Fe-26Cr-4.4C-4.8Ti-1Ni.

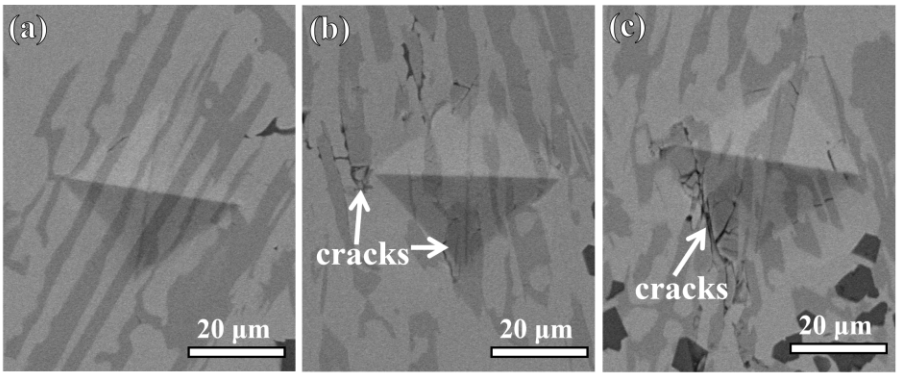

Fig. 12. SEM image of the indentations: (a) C3, (b) H2, and (c) H3.

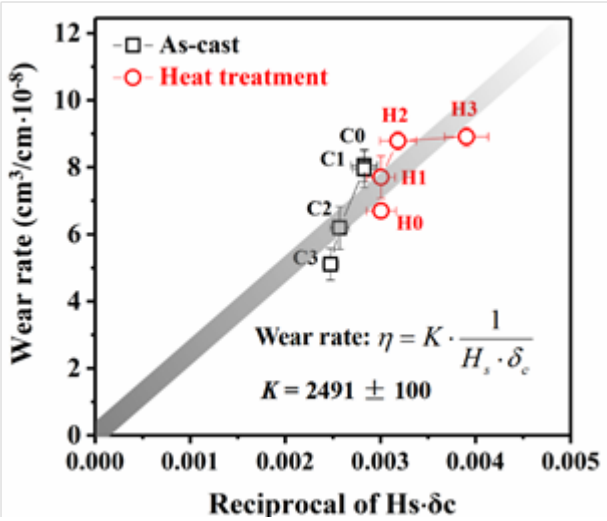

Fig. 13. Change of wear rate with the scratch properties of the composites.